AVO analyses of reflected seismic data over sand-filled channels

Taiwen Chen and Donald C. Lawton

ABSTRACT

Seismic reflection data over a sand-filled channel in southern Alberta and acoustic seismic reflection data over a physical model of a channel system typical of those found in the same area have been obtained. These data have been processed and studied in terms of Amplitude Versus Offset (AVO) behavior. There appear to be no pronounced AVO effect for these channels. Synthetic data were also generated to analyse the AVO effects.

INTRODUCTION

The study of variation in reflection amplitude with source-receiver offset (AVO) has been proposed by many authors (Ostrander, 1984: Wren, 1984: Rutherford, 1989). Ostrander used a three-layer gas sand model, the gas sands that produce the amplitude anomalies have lower impedance than the encasing shales and have reflections that increase in magnitude with offset. He concluded that Poisson's ratio has a strong influence on changes in reflection coefficient as a function of angle of incidence and the the analysis of seismic reflection amplitude versus shot-to-group offset can in many cases distinguish between gas-related amplitude anomalies and other types of amplitude anomalies. Rutherford developed the Ostrander's idea. He grouped gas-sand reflectors into three classes defined in terms of R_0 at the top of the gas sand: class 1 gas sands have higher impedance than the encasing sediments, class 2 have the same impedance as the encasing sediments and class 3 have lower impedance than the encasing sediments (Ostrander's model is this class). Class 3 gas sands are often subjects of AVO analysis, for these sands are the easiest to find on stacked data and the S/N as a function of offset for these sands is usually adequate for AVO analysis.

In our study, the class 3 sands were studied to analyse their AVO effects. One line of P-P case seismic reflection data was obtained in Southern Alberta. In this area, channel sandstones of the Glauconitic member of the Lower Mannville Formation are good exploration targets. These channels are generally less than 30 m thick, whereas the dominant wavelength of typical reflection data is rarely less than about 80 m. The line was processed and analysed for AVO effects.

In 1989, CREWES Project at University of Calgary developed a tank model of a sand-filled channel based on a typical southern Alberta channel system environment, in order to study AVO effects over thinly bedded sequences. The processing results are also discussed in this paper. Numerical seimic data were also obtained and studied in terms of the AVO effects.

ENCHANT FIELD SEISMIC DATA

Figure 1 shows the study area, from which one seismic line (82-227, Enchant) was provided for this study. Table 1 summarizes the acquisition parameters, and an example of a shot gather is shown in Figure 2. The goal of data processing for AVO was to preserve amplitude variation with offset while removing the effects of spherical spreading, attenuation, transmission loss, and other propagation factors.

The processing flow for line 82-227 is outlined in Table 2, and Figure 3 shows the final stacked section of the line. In Figure 3, "M" is Mississippian, "D" is Devonian, "P_{ϵ}" is PreCambrian (basement). The zone of interest from about 700 ms to 750 ms is boxed in. The channel can be clearly seen, from CDP 590 to CDP 630, and it is about 500 m wide.

TANK SEISMIC DATA

Model construction

A channel model 0.6 m square was constructed out of plexiglas, plaster of Paris and steel, and it was put in the modelling tank (Figure 4), which was full of water. Hence only P-wave data were received. The whole recording procedure was controlled by IBM XT system. The plaster constitutes the low-velocity fill in channels that were milled from a plexiglas layer 0.6 cm thick. A plan view of the model is shown in Figure 5.

The distance and time scale factors for the model are 1:5,000, so the model represents a 3 km x 3 km area after scaling. Channel 1 has a uniform thickness of 31 m (scaled) whereas channel 2 is primarily 15 m thick. Channel margins with the heavy outline in Figure 5 were bevelled at 45 degrees and the remaining margins were left as vertical cut-banks. The stratigraphy of the model is shown Table 3.

Data acquisition

One line of multichannel data was collected along 65 of the model (Figure 5). The line contained 40 records, each record consisting of 120 traces, with a near offset of 100 m, a far offset of 1280 m, and a group interval of 20 m, yielding 15-fold subsurface coverage. An example of a shot gather from the data set is shown in Figure 6. This record was taken with the shot point located between channel 1 and channel 2, and the channel events are clearly visible in the data.

Data processing

Tank data processing is rather simple compared with the field data. For example, the velocities are known, so there is no need to undertake the velocity analysis. Table 4 shows the processing flow used for the tank data.

Figure 7 is the stacked section of the tank data. The S/N ratio is high and three channels are clearly seen. Channel 1, from CDP 193-223 (300-310 m wide); channel 2 from CDP 263-280 (170 m wide), 353-400 (470 m wide), respectively. The errors are between 0 - 40 m.

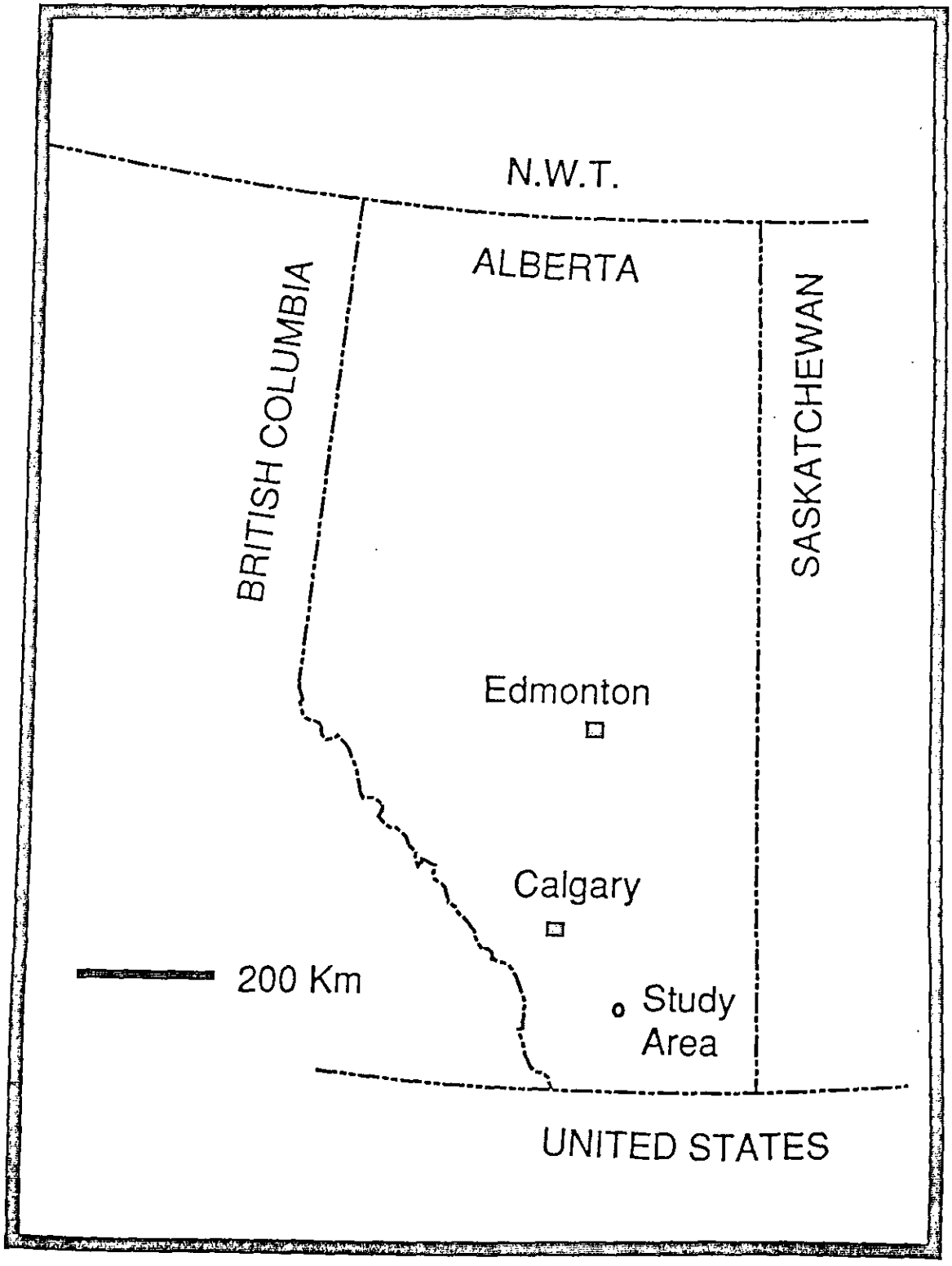

Figure 1: Location of study area.

TABLE 1: FIELD ACQUISITION AND RECORDING PARAMETERS FOR LINE 82-227 OF THE ENCHANT SURVEY.

Source:	Dynamite, 1 kg, depth 15 m
Geophones per group:	10
Type of geophones used:	Geosource 20-D
Spread:	Split-spread, 96 channels, with near offset 25 m and far offset 1200 m
Group interval:	25 m
Normal source interval:	150 m
Fold:	8
Recorded format:	SEG-B
Recorded length:	3 sec
Sample rate:	2 ms
Field filter:	Low cut: 15 hz Low-cutoff of slope: 36 db/oc High cut: 125 hz High-cutoff of slop: 72 db/oc Notch: in

TABLE 2: PROCESSING SEQUENCE FOR LINE 82-227 OF THE ENCHANT SURVEY.

DEMULTIPLEX
GEOMETRY
    Geometric spreading compensation, transmission losses, inelastic attenuation, trace balance, elevation statics
SPIKING DECONVOLUTION
    80 ms length operator, 0.1% prewhitening
CDP SORT
REFRACTION STATICS
INITIAL VELOCITY ANALYSIS
AUTOMATIC SURFACE-CONSISTENT STATICS
    Correction window from 250 to 2000 ms,
    maximum shift of + or - 16 ms
BANDPASS FILTER
    Zero phase, 12/24 - 70/48
MUTE
RMS GAIN
    Window from 400 to 2200 ms
FINAL VELOCITY ANALYSIS
NMO
CDP TRIM STATICS
    Correction window from 300 to 1300 ms
    Maximum shift of + or - 12 ms
AVA TRACES

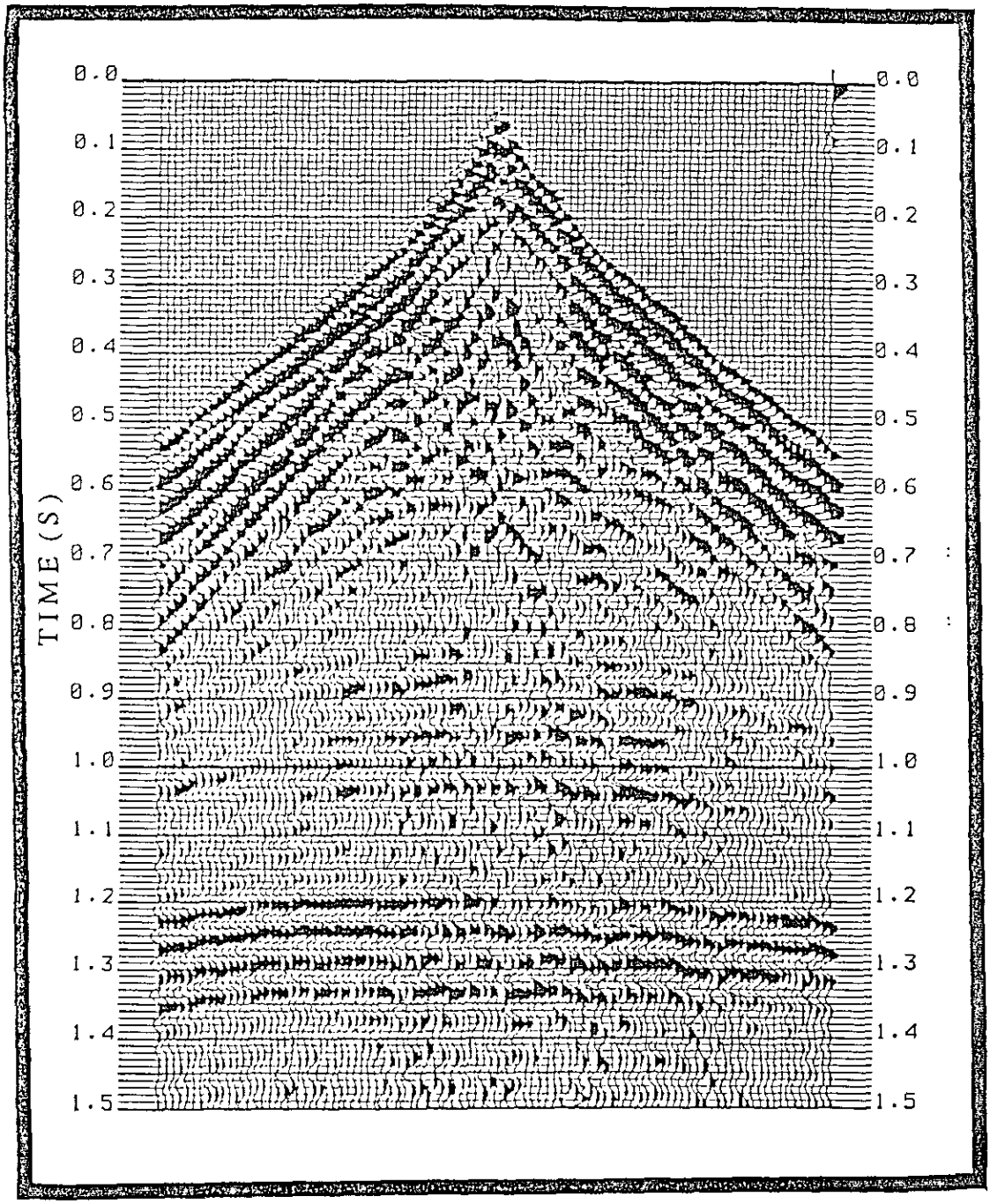

Figure 2: Example of a shot gather from Line 82-227, Enchant. The Mannville channel occurs at about 0.8 s.

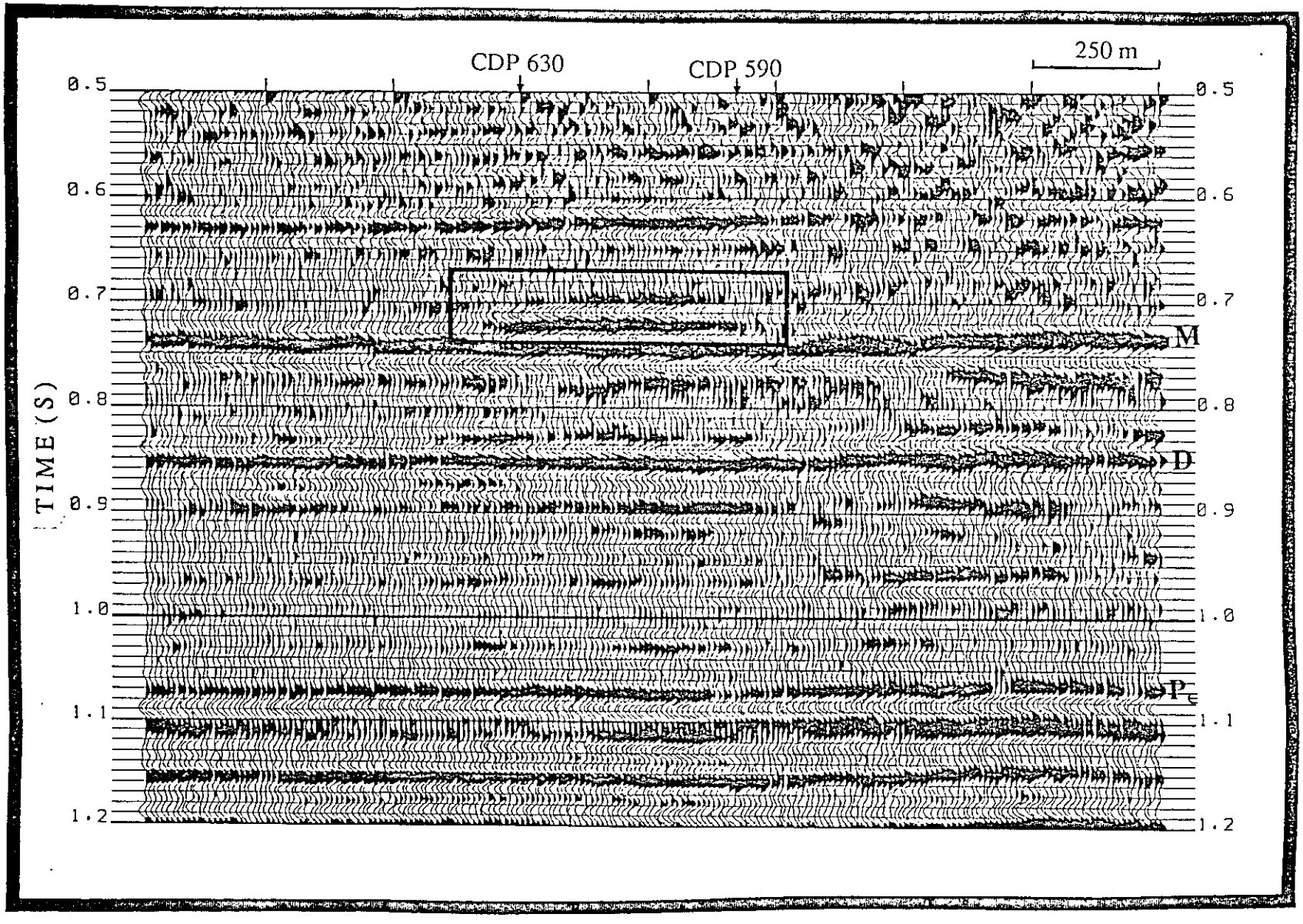

Figure 3: Stacked section after trimstatics, Line 82-227, Enchant.

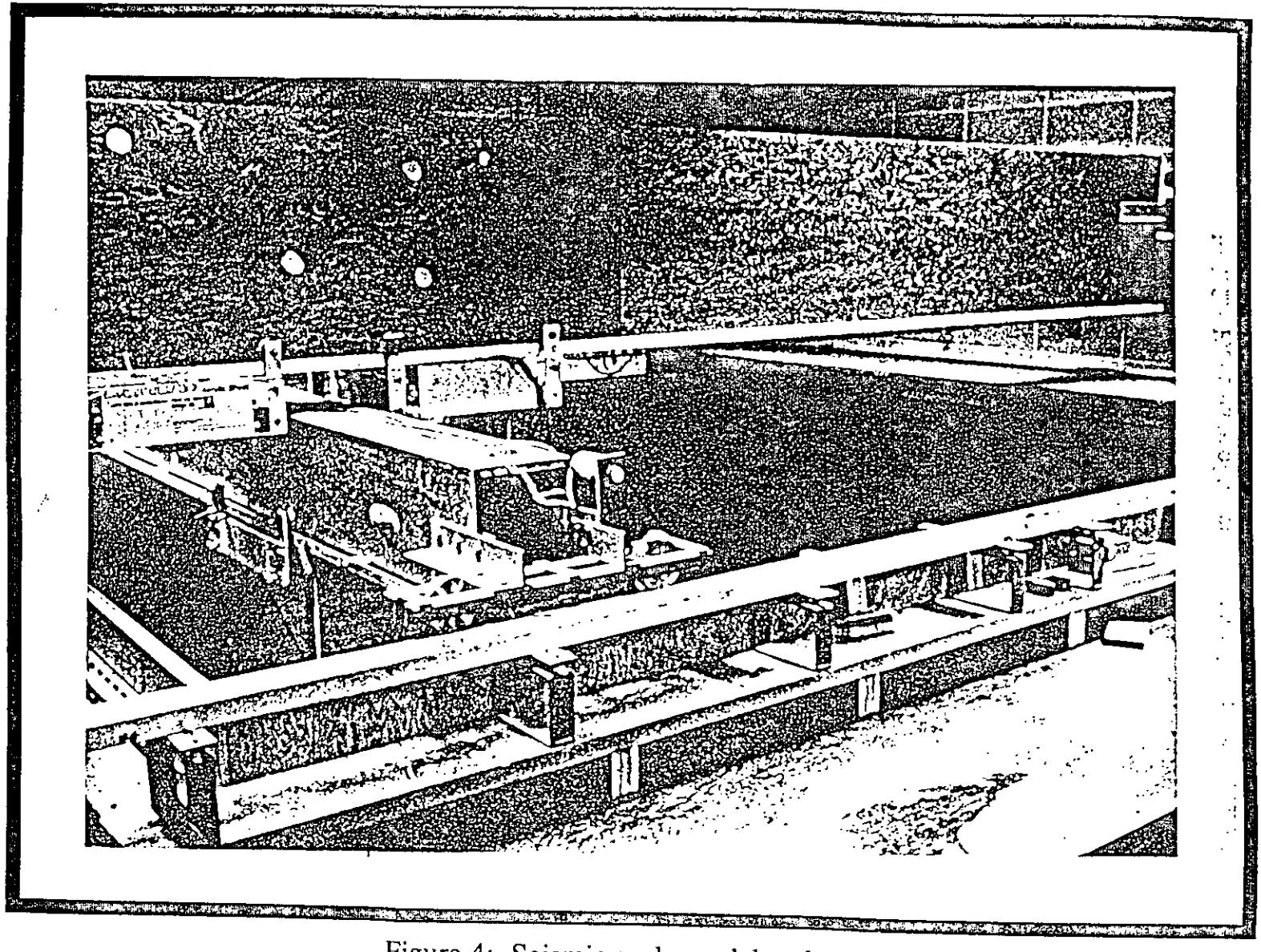

Figure 4: Seismic scale model tank.

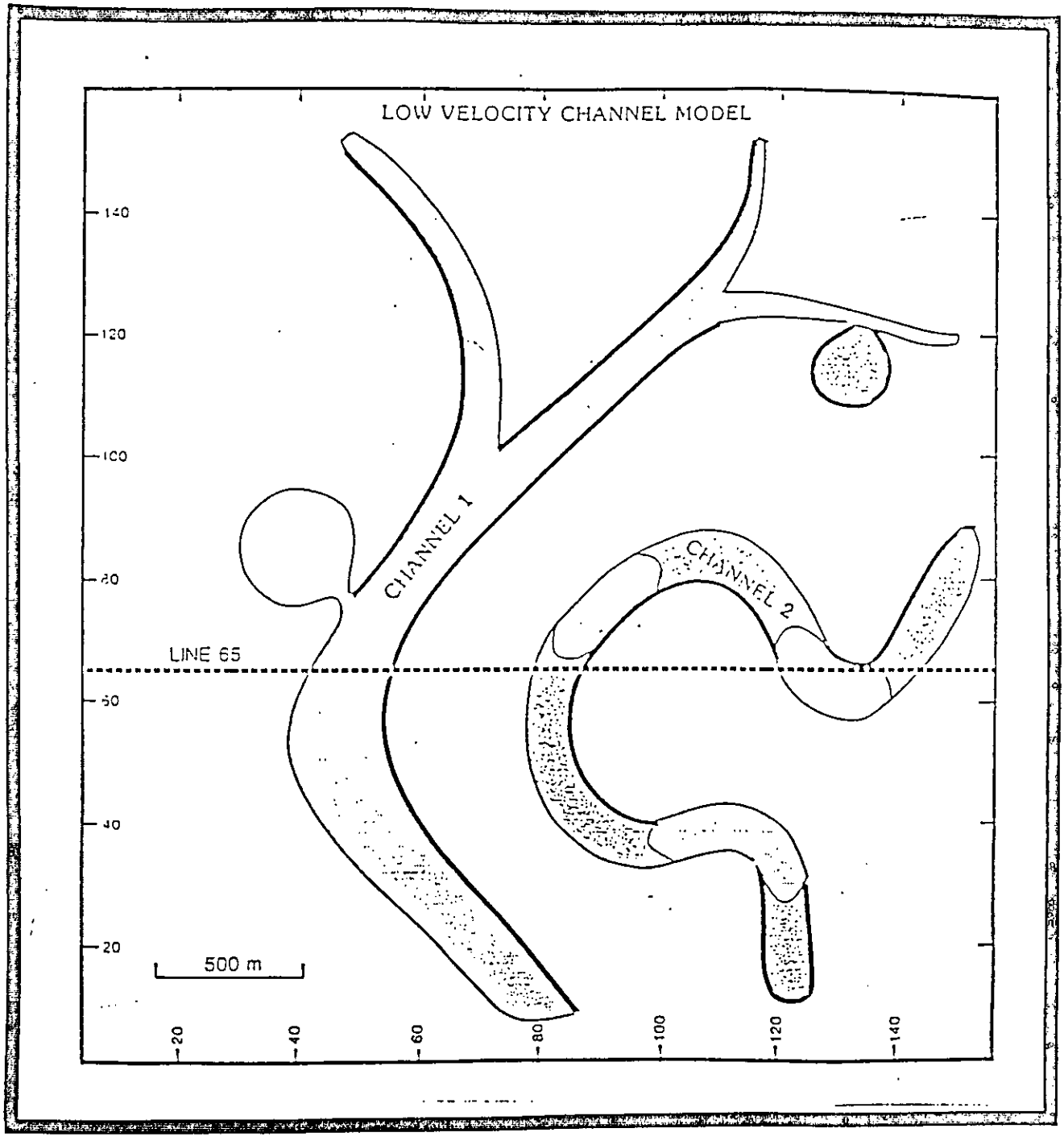

Figure 5: Plan view of the channel model (Lawton et al, 1989).

TABLE 3: VERTICAL SECTION THROUGH CHANNEL 1 OF THE TANK MODEL.

Layer	Compound	Thickness (actual,cm)	Thickness (scaled,m)	Vp (m/s)	Vs (m/s)	σ	ρ (g/cm^3)
1	Plexiglas	5.08	254	2740	1385	0.33	1.20
2	Plaster	0.63	31	2150	1180	0.28	1.14
3	Plexiglas	0.95	48	2740	1385	0.33	1.20
4	Steel	1.59	80	5800	3300	0.26	7.80

TABLE 4: TANK DATA PROCESSING SEQUENCE.

DEMULTIPLEX
GEOMETRY
CDP SORT
NMO
CDP TRIM STATICS
Correction window from 1150 ms to 1250 ms, Maximum shift of + or - 12 ms
AVA TRACES

TABLE 5: THE PARAMETERS USED IN SIERRA MODEL.

Layer	Depth (m)	Vp (m/s)	Vs (m/s)	σ	ρ
1	850	1480	1	0.50	1.00
2	1104	2740	1438	0.31	1.20
3	1136	2000	1237	0.19	1.14
4	1184	2740	1438	0.31	1.20
5	1263	5800	3349	0.25	7.80
6	2000	1480	1	0.50	1.00
HS		9144	5279	0.25	3.03

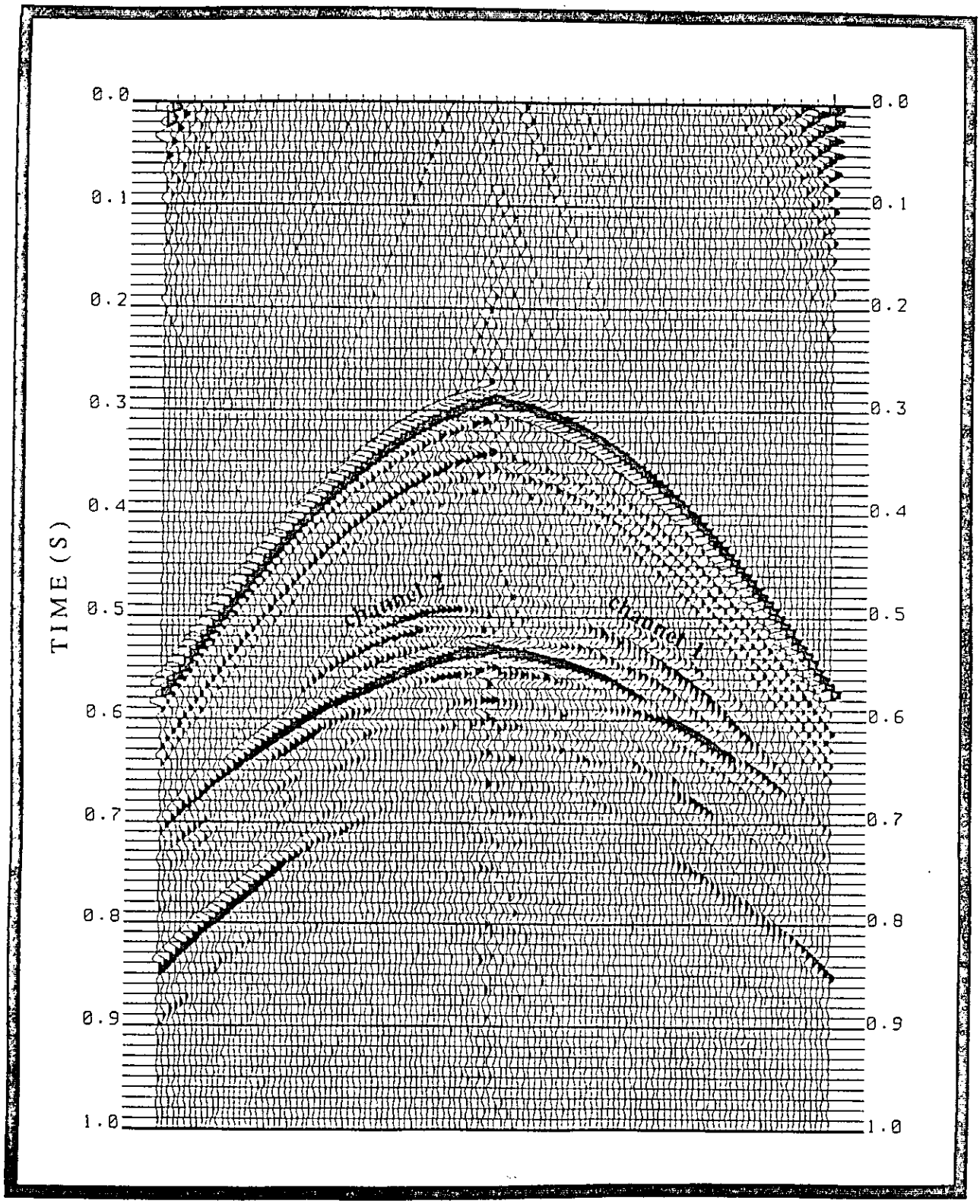

Figure 6: Example of a shot gather from Line 65, tank model, showing channel events.

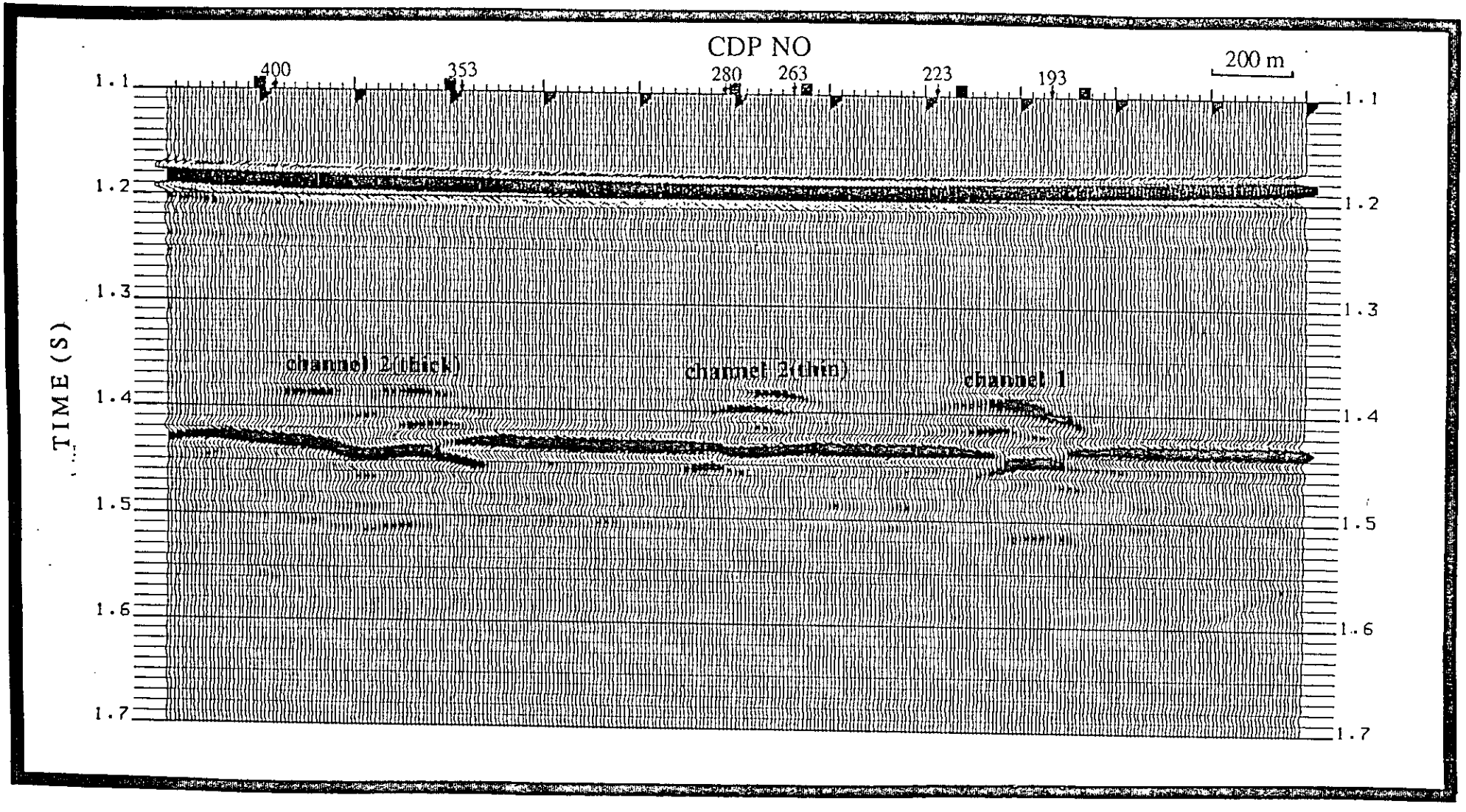

Figure 7: Stacked section after trimstatics, tank data.

SYNTHETIC SEISMIC DATA

A 2-D channel model was built (shown in Figure 8) using Sierra Package to mimic the tank model. Table 5 shows the physical parameters used for channel 1 in Sierra model. The same acquisition geometry was used as for the tank model: the line contains 40 shot records, each consisting of 120 traces, with near offset of 100 m and far offset of 1280 m, and a group interval of 20 m, yielding 15-fold subsurface coverage. Figure 9 shows one shot gather, in which channel 1 and channel 2 are both clearly seen. The same processing sequence was used as for the tank data, and Figure 10 is the final stacked section.

AVO ANALYSIS

Figure 11 shows a CDP gather (CDP 600) from over the channel of the processed field data. By ray tracing, it is possible to determine the angel and position from which each sample of a trace comes from, then it is possible to group all samples from the same reflection and similar angles of incidence, thus producing gather of Amplitude-Versus-Angle (AVA). Figure 12 is AVA traces of CDP 600. From Figure 11 and Figure 12, it can be concluded that there is no pronounced AVO effects for the channel events.

Figure 13 shows a CDP (CDP 211) from over the channel 1 of the tank data. Figure 14 is Amplitude-Versus-Angle traces of CDP 211. From Figure 13 and Figure 14, it is obvious that there is no pronounced AVO effects for the channel events, although the Mississippian event (labelled as 'M' in these Figures) shows a strong amplitude decrease with offset .

Figure 15 shows a CDP (CDP 214) from over the channel 1 of the Sierra data. Figure 16 is Amplitude-Versus-Angle traces of CDP 214. From Figure 15 and Figure 16, it also can be concluded that there is no pronounced AVO effects for the channel events.

AVO is an effective way to distinguish between gas-related amplitude anomalies and nongas related anomalies. Unfortunately, there are a lot of major factors which affect the recorded amplitude of a reflection as a function of offset, such as spherical spreading, event tuning (thin bed effect) and inelastic attenuation (Ostrander, 1984). This paper will not discuss these factors, even some of them were considered during the processing.

For the tank data, the R_0 (normal incidence reflection coefficient) for the top of the channel can be obtained by:

$$R_0(t)=(\alpha_2\rho_2-\alpha_1\rho_1)/(\alpha_2\rho_2+\alpha_1\rho_1)=(2150 \times 1.14-2740 \times 1.2)/(2150 \times 1.14+2740 \times 1.20)=-0.15$$

R_0 in Ostrander's model:

$$R_0(o)=(\alpha_2\rho_2-\alpha_1\rho_1)/(\alpha_2\rho_2+\alpha_1\rho_1)=(8000 \times 2.14-10000 \times 2.4)/(8000 \times 1.24+10000 \times 2.4)=-0.17$$

$$R_0(t)\approx R_0(o)$$

and the Poisson's ratio for the channel events is smaller than the encasing rocks, same as Ostrander's gas sand model and the third class of Rutherford's. For the tank data, the amplitude of both the top and the bottom of the channels should increase when the offset gets larger, as Ostrander's results (Figure 17).

It is known that $\Delta\sigma$ contributes most significantly to $R(\theta)$ (Shuey). For moderate angles of incidence, the relative change in reflection coefficient is particularly significant when Poisson's ratio differ greatly between the two media (Ostrander, 1984). Poisson's ratio difference between the channel and the encasing rock of the tank data is:

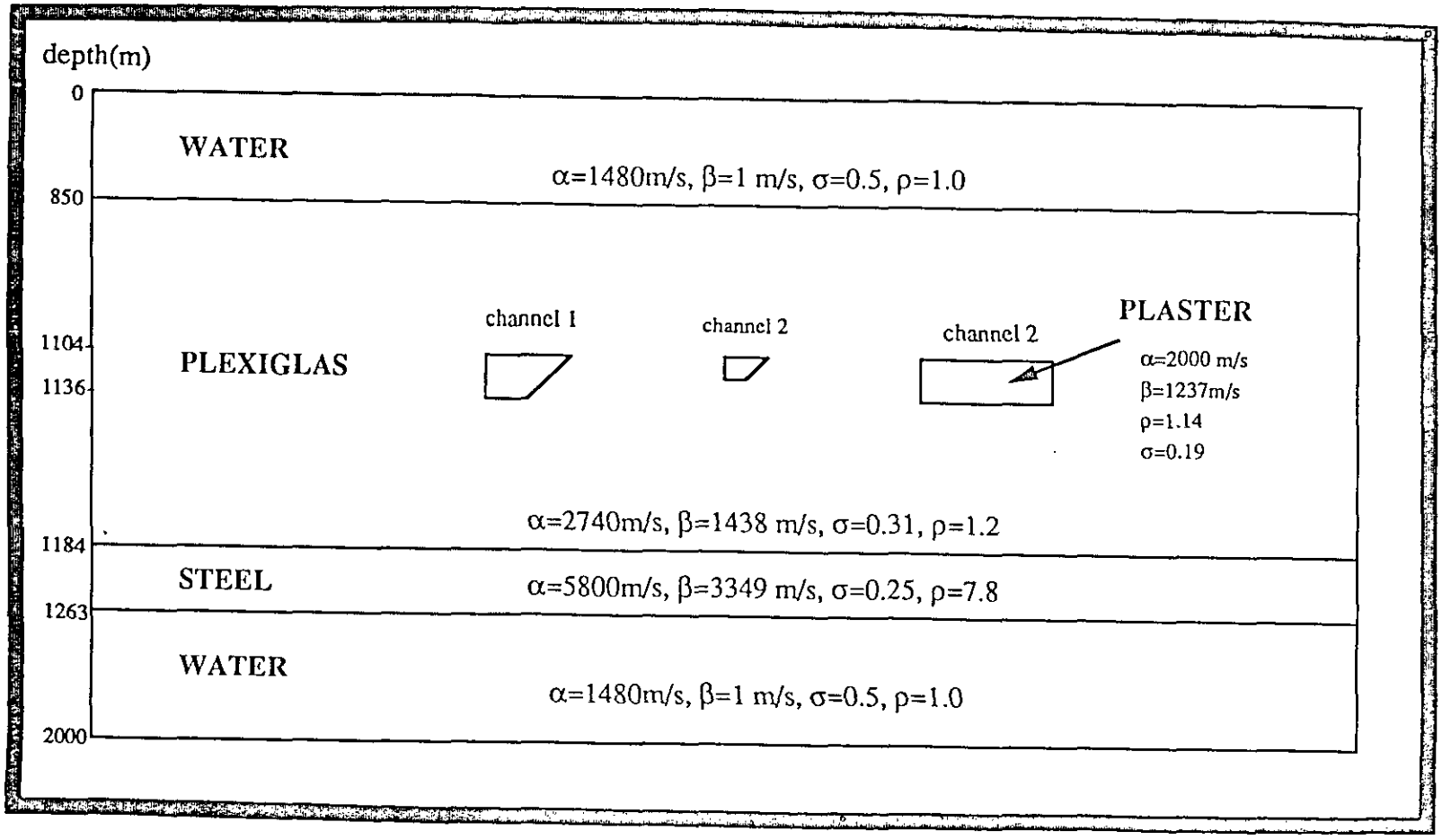

Figure 8: 2-D model built in Sierra Package (not to scale).

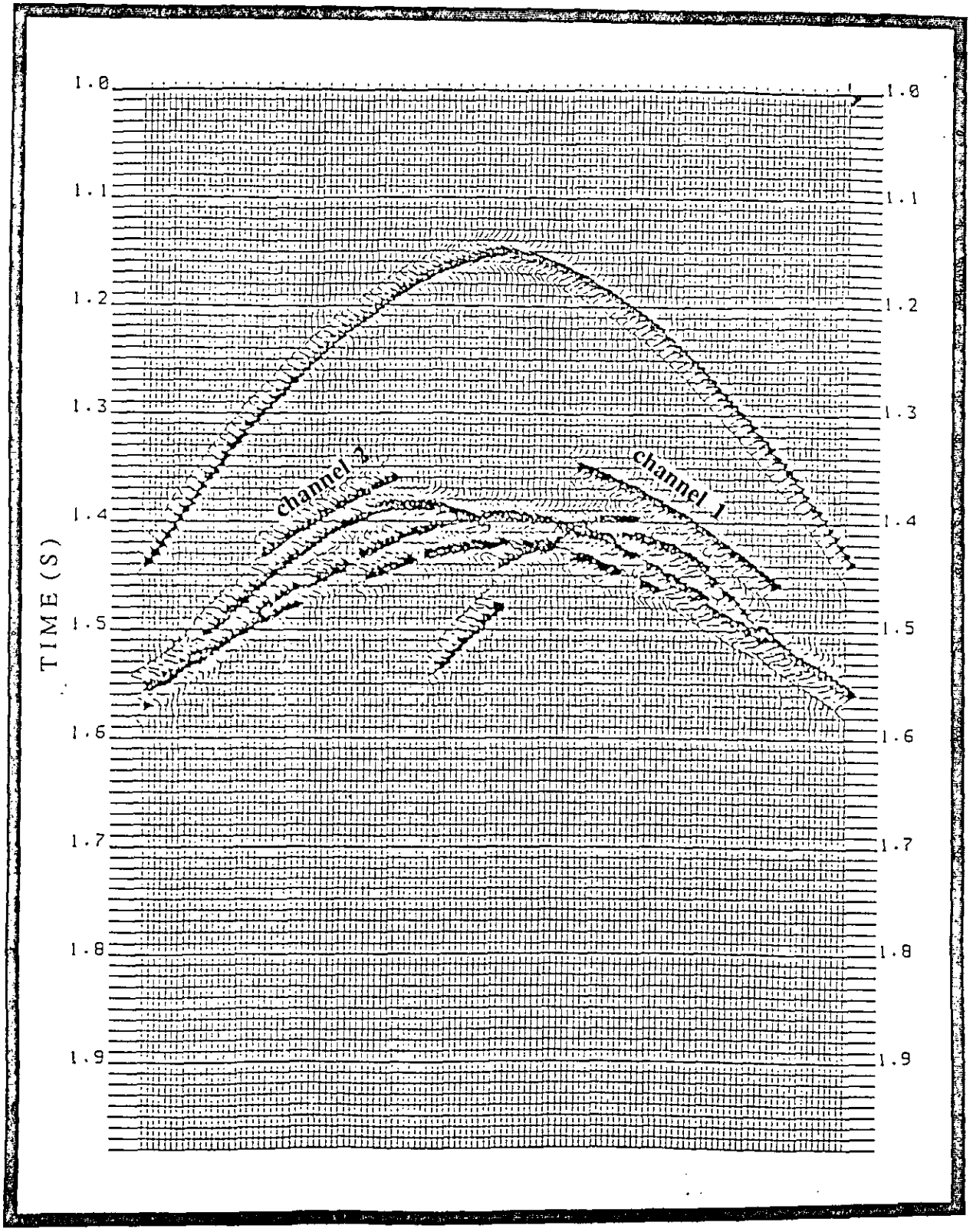

Figure 9: Example of a shot gather, Sierra Package.

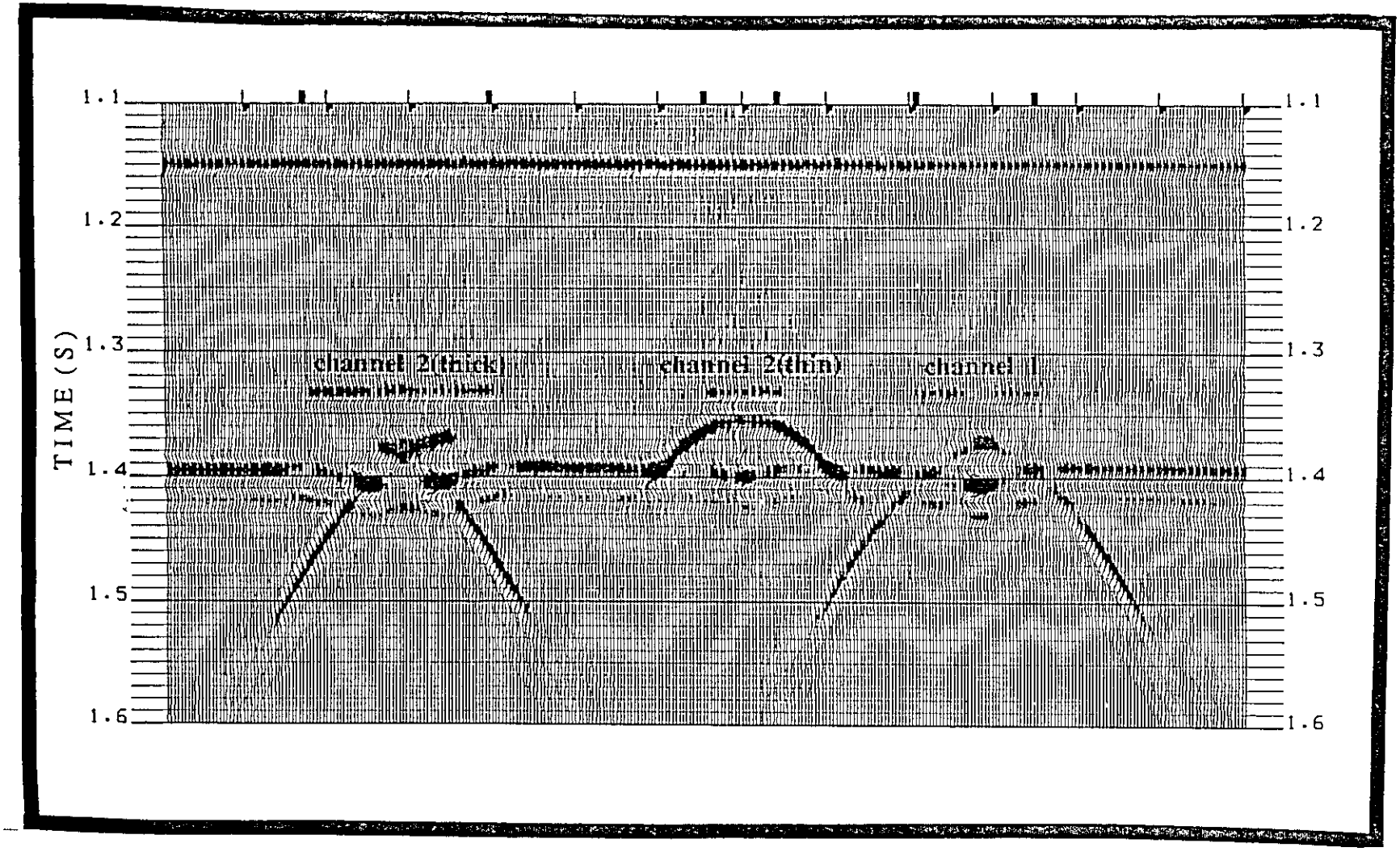

Figure 10: Stacked section after trimstatics, Sierra Package.

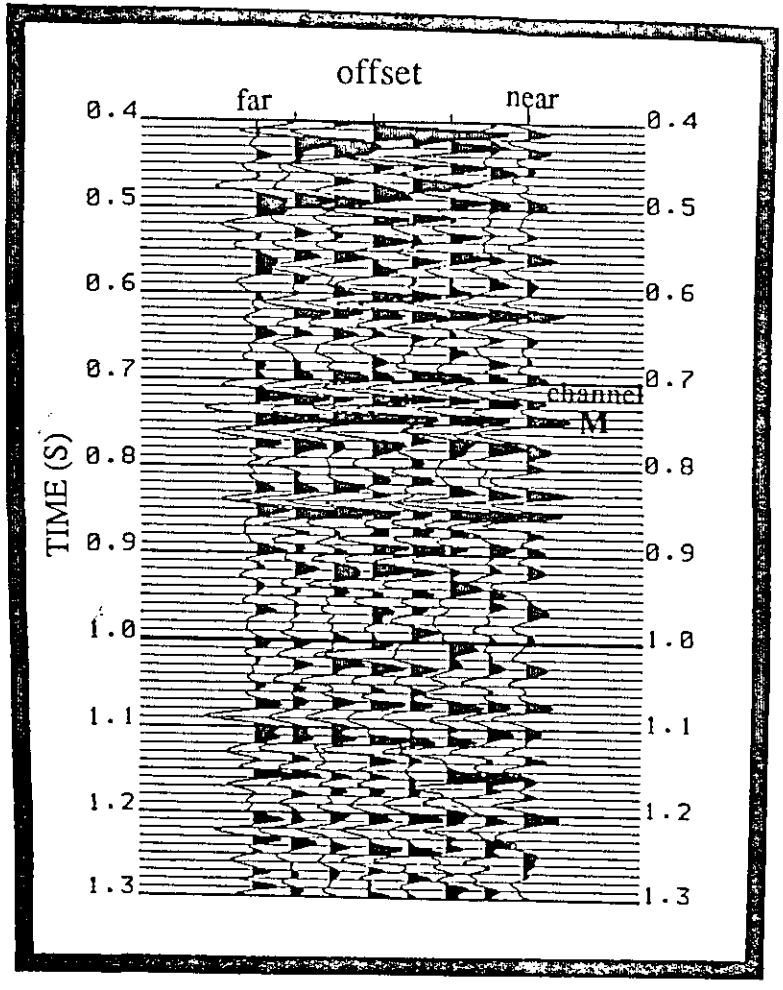

Figure 11: CDP 600, after trimstatics, Line 82-227, Enchant.

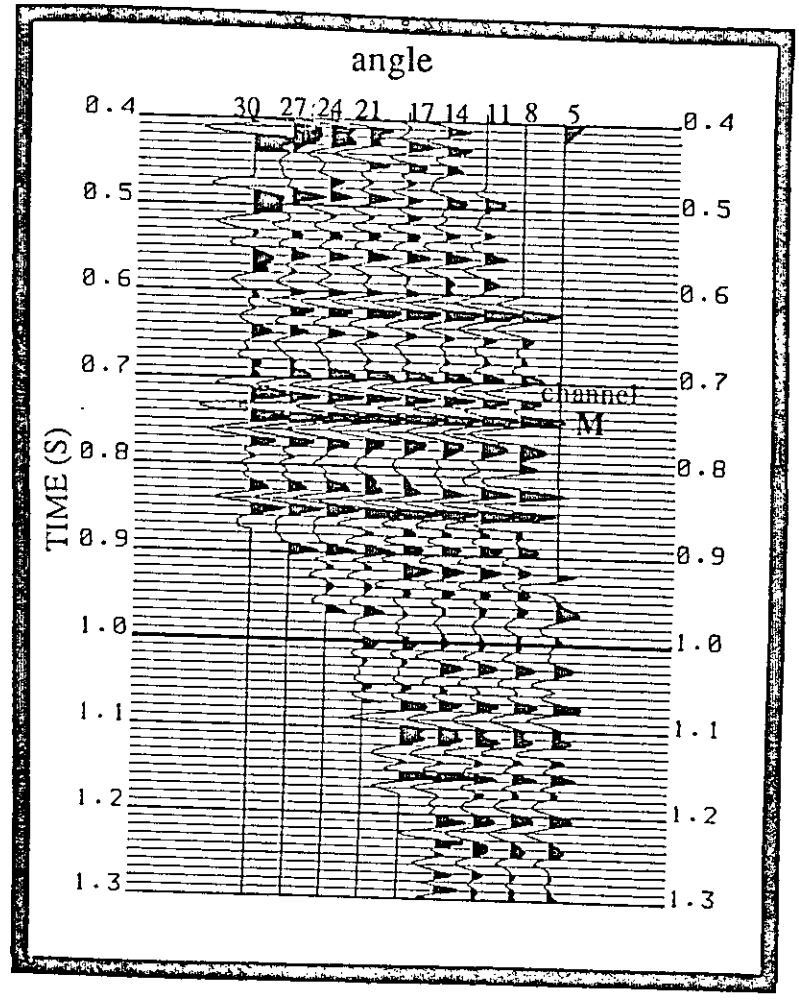

Figure 12: AVA traces of CDP 600, Line 82-227, Enchant.

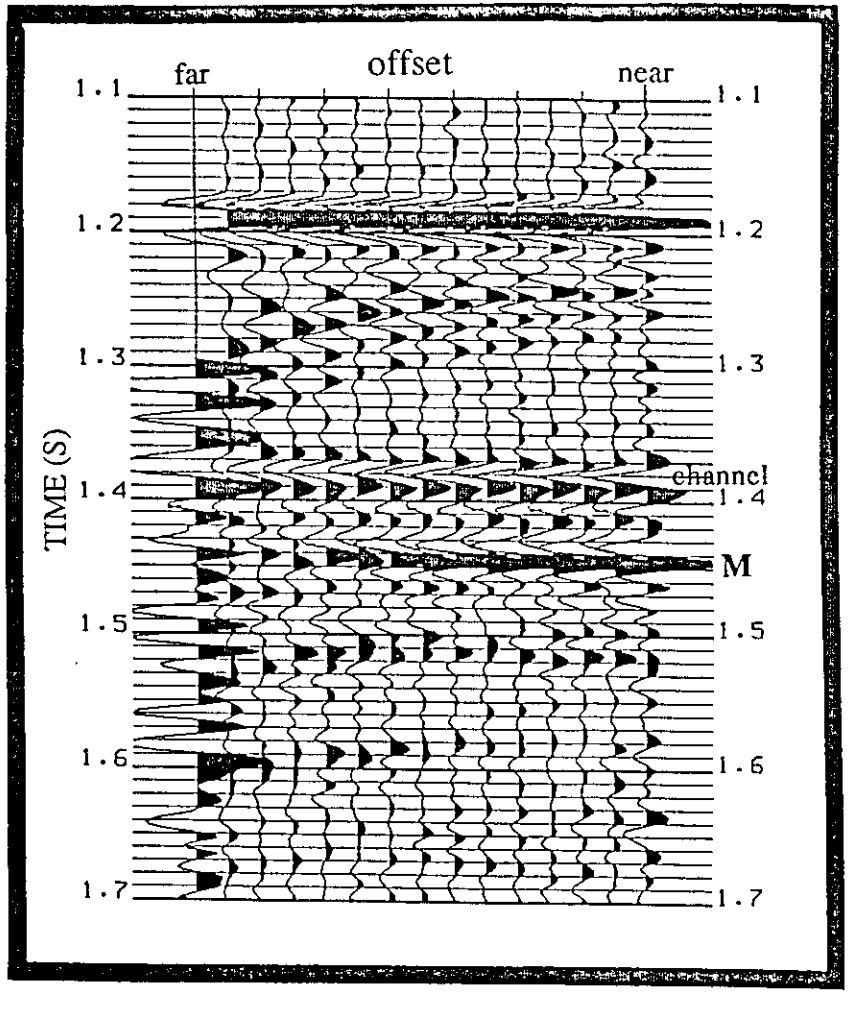

Figure 13: CDP 211, after trimstatics, tank data.

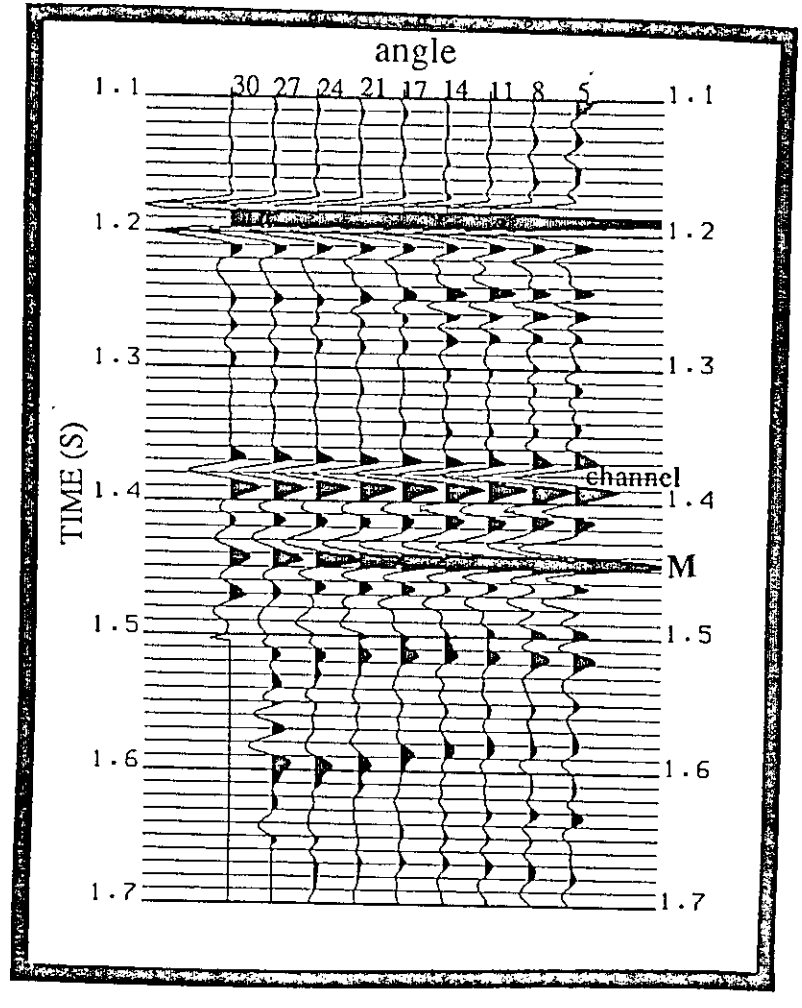

Figure 14: AVA traces of CDP 211, tank data.

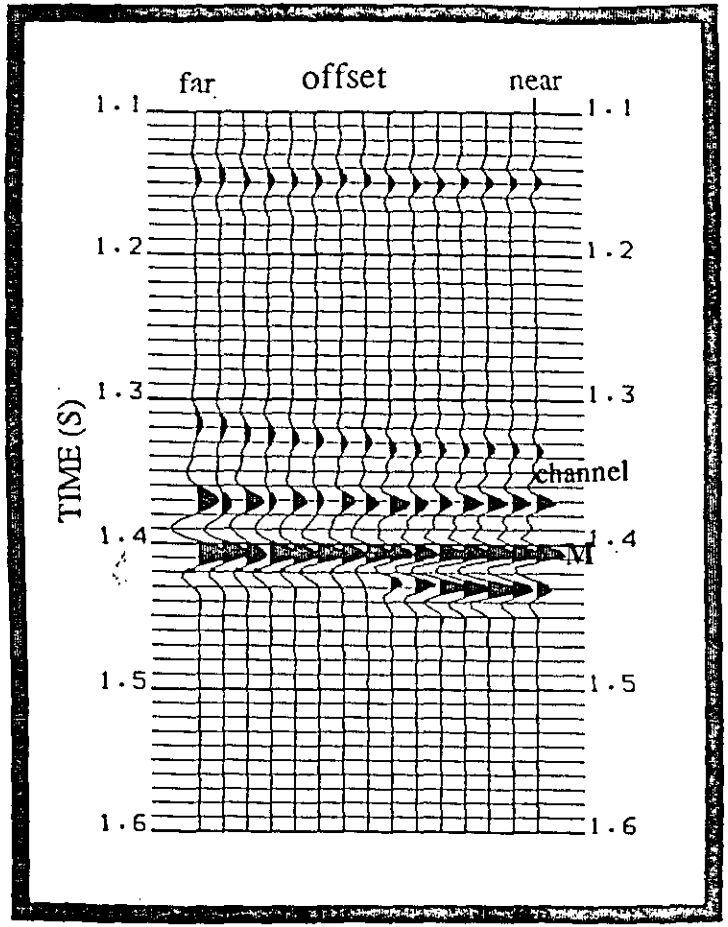

Figure 15: CDP 214, after trimstatics, Sierra Package data.

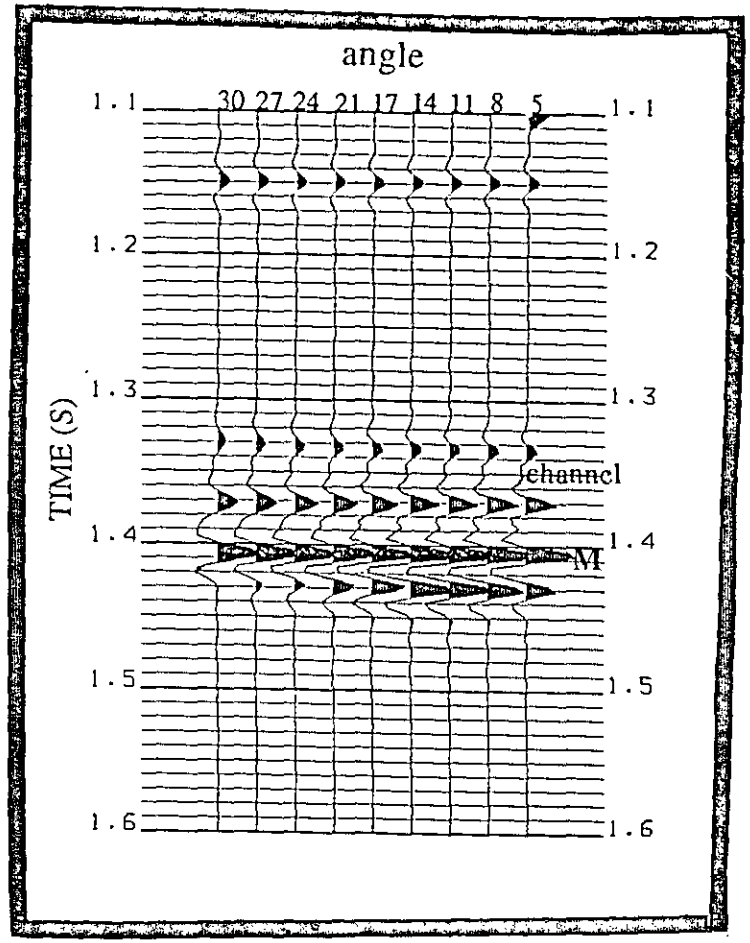

Figure 16: AVA traces of CDP 214, Sierra Package data.

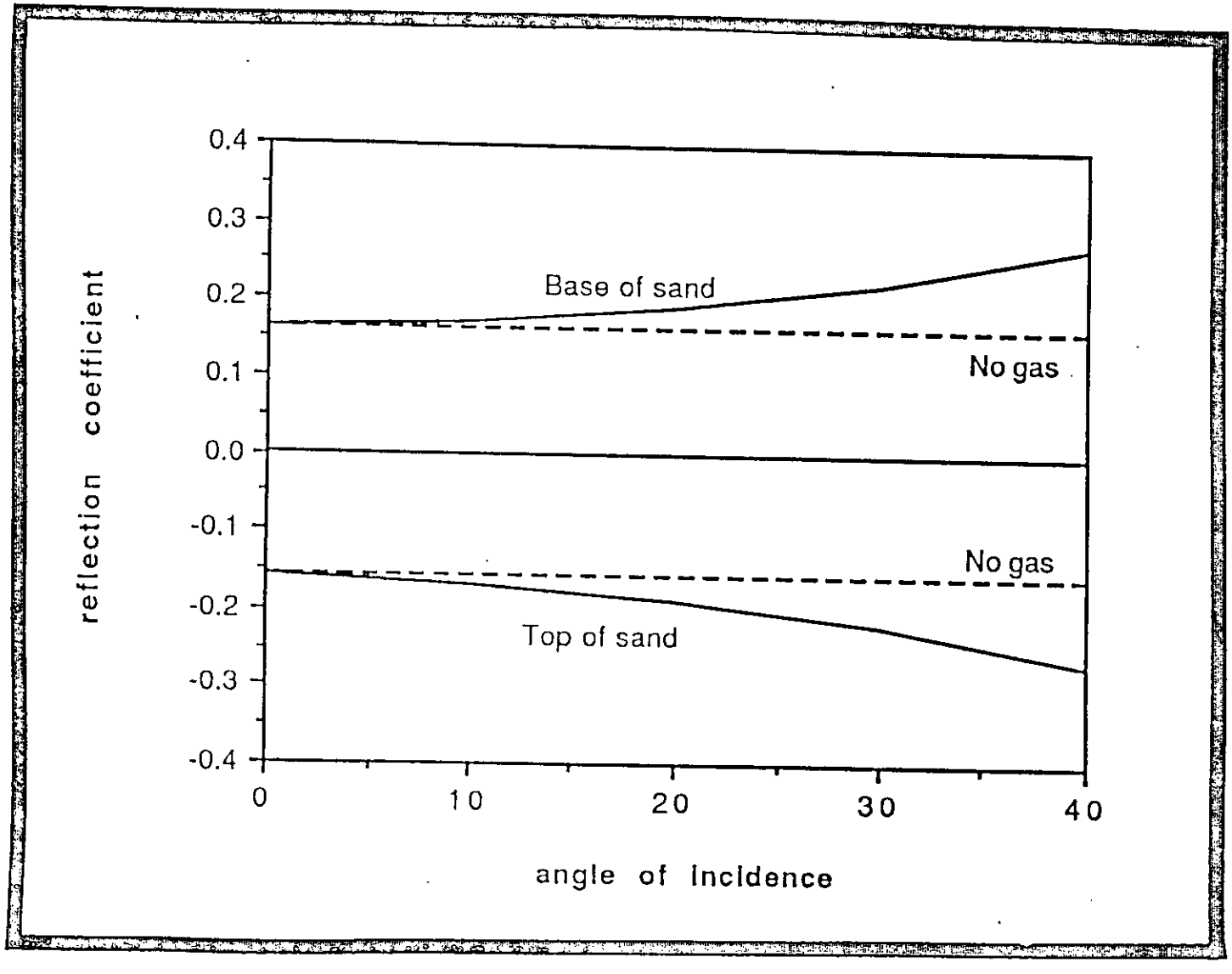

Figure 17: Plot of P-wave reflection coefficients versus angle of incidence for three-layer gas sand model (after Ostrander, 1984).

$\Delta\sigma$=0.33-0.28=0.05

and $\Delta\sigma$ for Ostrander's model is:

$\Delta\sigma$=0.40-0.10=0.30

The $\Delta\sigma$ used in tank model is much smaller than that in Ostrander's model.

Additional modelling was undertaken using the Hampson-Russell AVO Package. There are several log well data available in study area, and only two wells were chosen for analysis. Well 6-1-13-19 is on-channel, and well 6-35-12-19 off-channel.

Figure 18 is the synthetic data for well 6-1-13-19, using sonic and density logs, without transmission losses, without geometrical spreading, no array effects, plane wave, 45 hz 100 ms Ricker wavelet, and the Poisson's ratio for the channel and the encasing rock are 0.20 and 0.32, respectively. Figure 19 is the synthetic data for the same well, using the same parameters except having transmission losses and with geometrical spreading. From Figure 18 and Figure 19, it can be said that there is only a small AVO effect for synthetic data considering the transmission and geometrical spreading.

$\Delta\sigma$ was changed to 0.3 for the well 6-1-13-19. The result is shown in Figure 20 (same parameters as in Figure 19 except $\Delta\sigma$). As we expect, the amplitudes of both the top and the bottom of the channel increase with increase in offset. The same $\Delta\sigma$ was used for well 16-35-12-19, Figure 21 is the synthetic data, without transmission losses, without geometrical spreading, no array effect, plane wave, 45 hz Ricker wavelet. Obviously, there is no AVO effect for the reflection events (marked with "A" in Figure 21) which correspond to the channel events in well 6-1-13-19.

DISCUSSION

From Figure 11 to Figure 16, the results for both the field data and model data are very similar: there are no pronounced AVO effects for the channel events. In these figures, "M" is Mississippian. In Figure 12 and Figure 16, there is no pronounced AVO effects for Mississippian event. However, in Figure 14 strong AVO effects can be clearly seen: the amplitude gets smaller after the angle of incidence gets larger for Mississippian. Steel was used in tank model to represent the Mississippian. For the boundary between Plexiglas and Steel, the reflection coefficient is positive, and the Poisson's ratio for the Steel is smaller than that for Plexiglas. This is the class 1 gas sand model discussed in Rutherford's paper, and the result from Figure 14 is the same as Rutherford's.

Comparing Figure 18 with Figure 19, it can be concluded that transmission losses and geometrical spreading do have a strong influence on the AVO effects. In Figure 20, after big $\Delta\sigma$ is used, the strong AVO effects can be seen on both the top and the bottom of the channel. In Figure 21, the same $\Delta\sigma$ is used, but no AVO effects are seen. From Figure 20 and Figure 21, it can be concluded that $\Delta\sigma$ does contribute much to the AVO effects, but not itself alone.

SUMMARY AND FUTURE WORK

Two basic conclusions can be got from this paper: (1): There is no AVO effects for the channel events of both field data and model data. For the tank data, the reason might mainly be the small reflection coefficient and small Poisson's ratio difference between the channel events and the encasing rocks. There is strong AVO effects for Mississippian in tank data due to the very large reflection impedance difference between Mississippian and

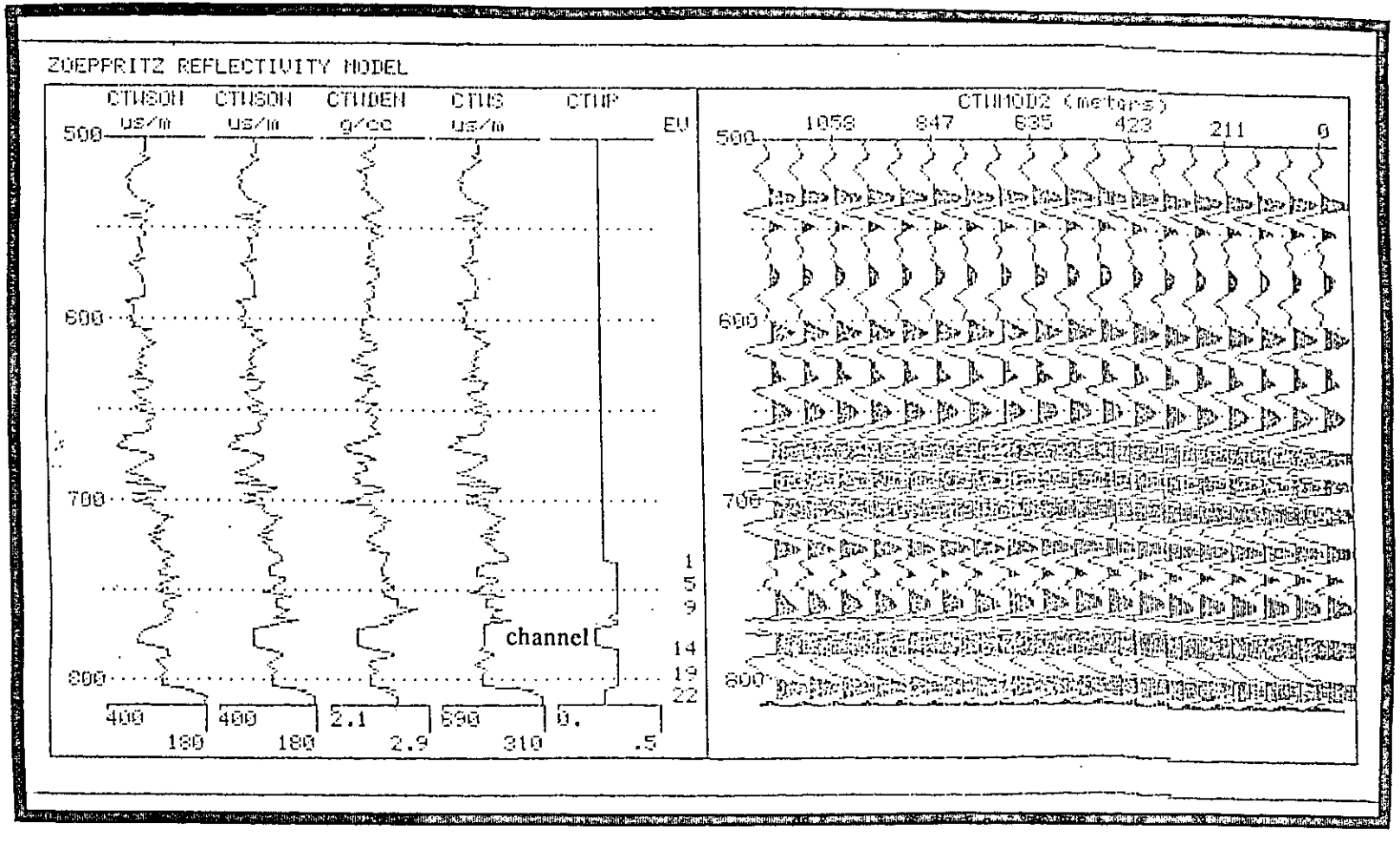

Figure 18: Synthetic data for well 6-1-13-19.

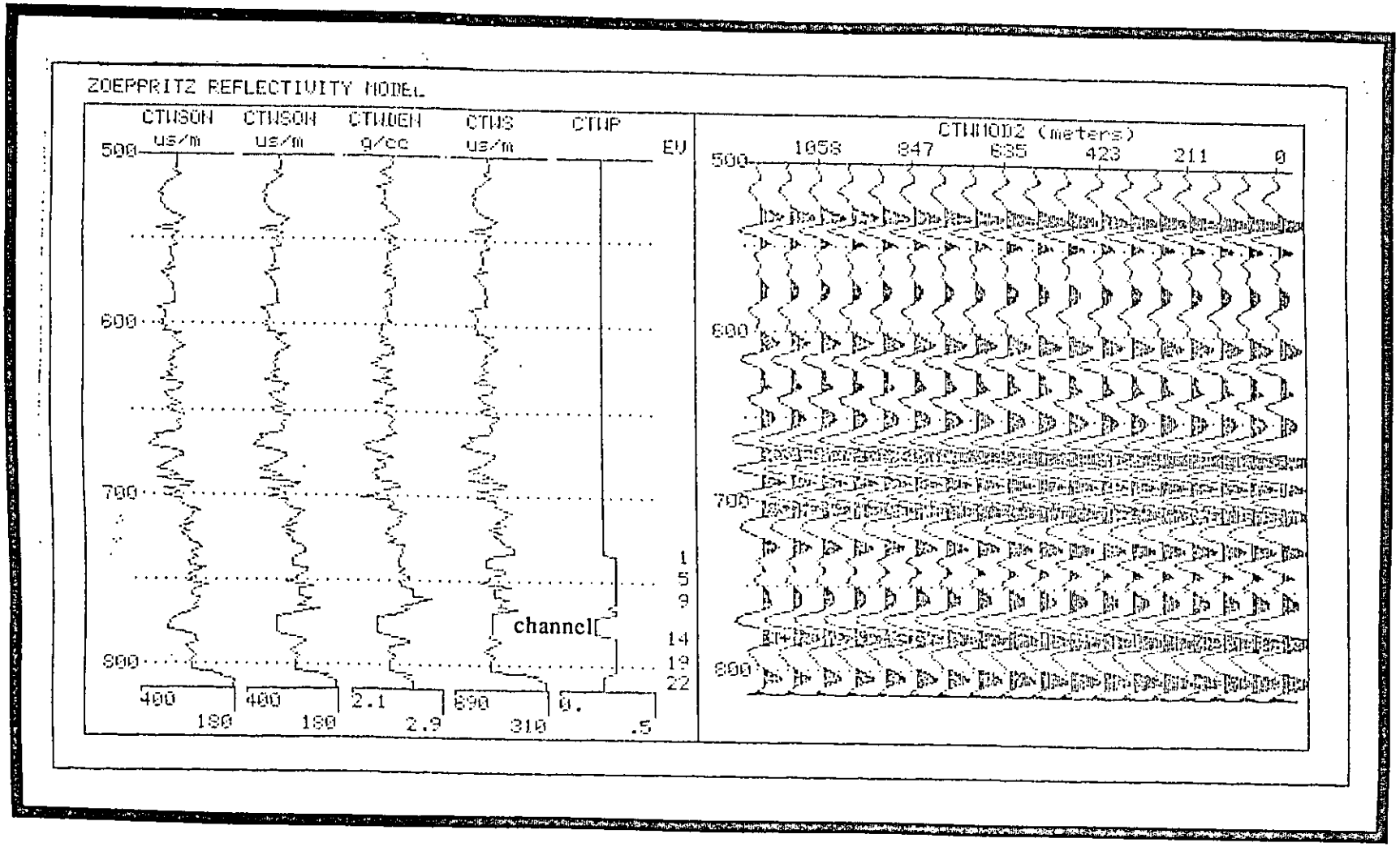

Figure 19: Synthetic data for well 6-1-13-19.

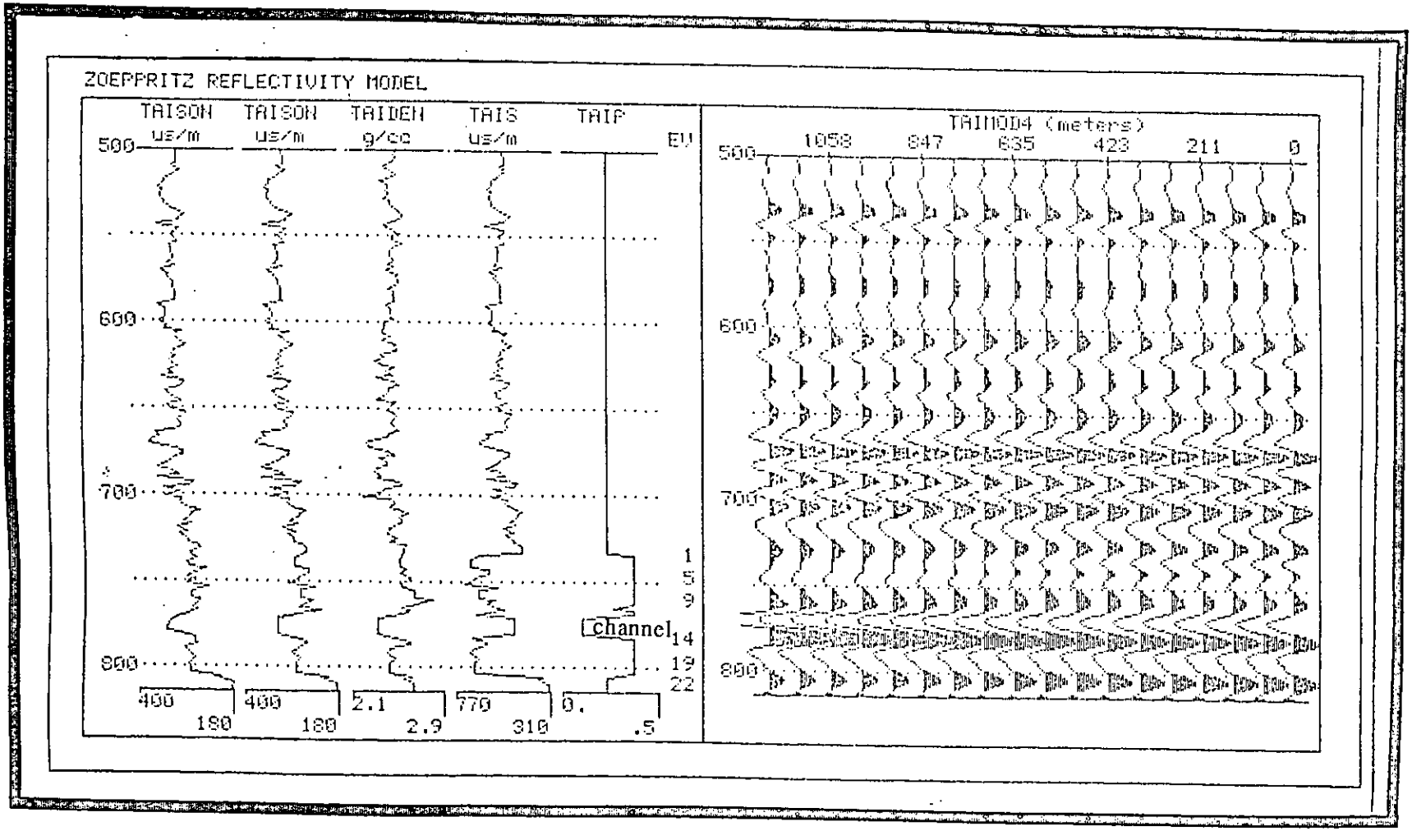

Figure 20: Synthetic data for well 6-1-13-19, $\Delta\sigma$=0.3.

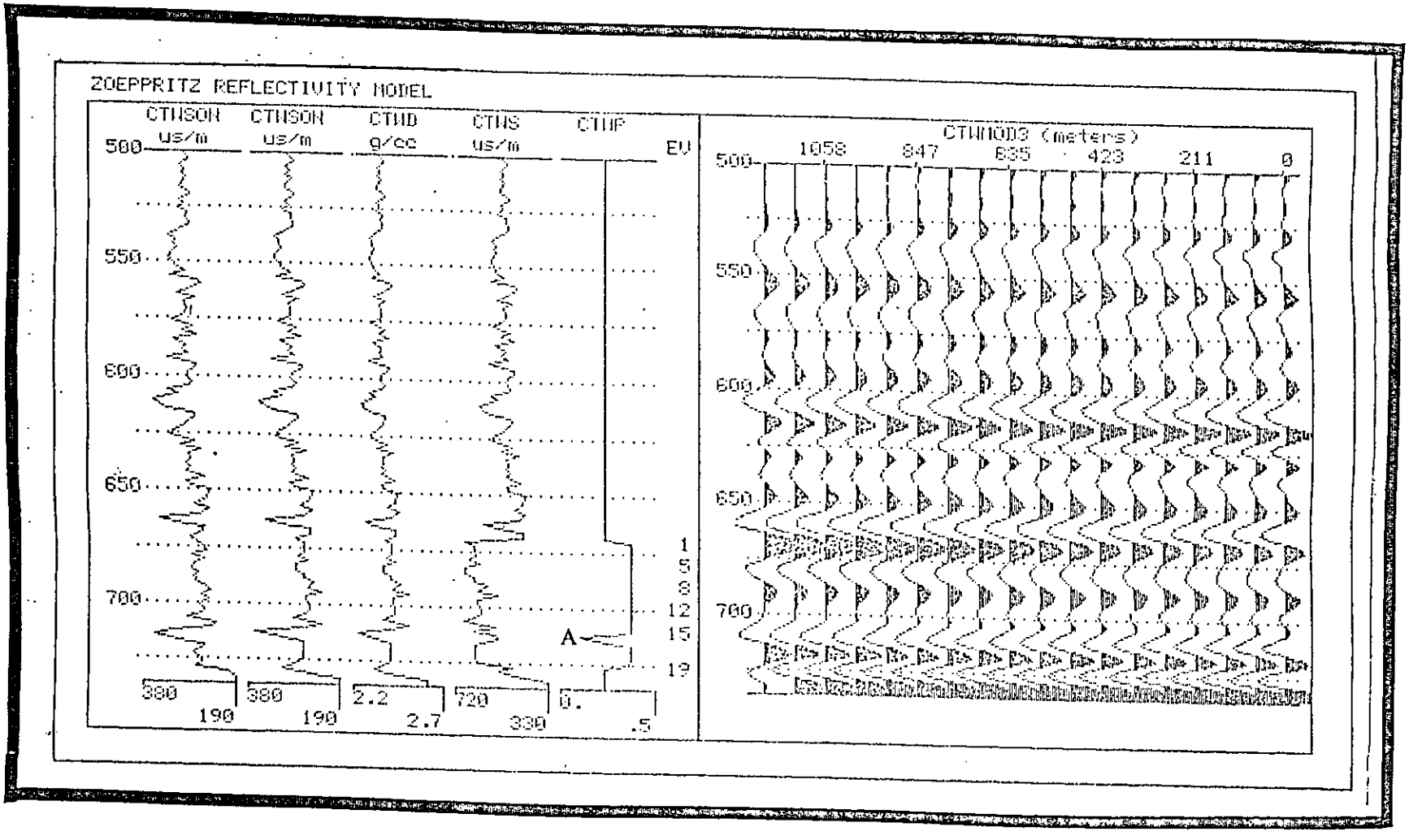

Figure 21: Synthetic data for well 16-35-12-19, $\Delta\sigma$=0.3.

the encasing rocks, and the Poisson's ratio difference exists too. (2): $\Delta\sigma$ contributes most significantly to $R(\theta)$, but not itself alone.

This work only includes P-P case. P-SV data will be analysed in terms of their Amplitude Versus Offset behavior. The affecting factors will also be discussed in the future work.

ACKNOWLEDGMENTS

We would like to thank CREWES Project for the support of this research and Tina Howell for her computer assistance. Special thanks to Shapiro Management Ltd. for contribution of the seismic data: Enchant line 82227.

REFERENCES

Harrison, M.P., 1989, Three-component seismic data processing: Carrot Creek, Alberta: University of Calgary, CREWES Project report, v. 1, 6-26.

Jain, S., 1987, Amplitude-Vs-Offset Analysis: A review with Reference to Application in Western Canada: J. Can. Soc. Expl. Geophys, v. 23, 27-36.

Lawton, D.C., Cheadle, S.P., Gallant, E.V., and Bertram, M.B., 1989, Physical seismic modelling of sand-filled channels: University of Calgary, CREWES Project report, v. 1, 342-344.

Neidell, S.N., 1986, Amplitude variation with offset: Geophysics: The Leading Edge of Exploration, March 1986.

Ostrander, W.J., 1984, Plane-wave reflection coefficients for gas sands st non-normal angles of incidence: Geophysics, v.49, no. 10, 1637-1648.

Rutherford, S.R. and Williams, R. H., 1989, Amplitude-Versus-Offset variation in gas sands: Geophysics, v. 54, no. 6, 680-688.

Shuey, R.T., 1985, A simplification of the Zoeppritz equations: Geophysics, v.50, 609-614.

Wren, A.E., 1984, Seismic techniques in Cardium exploration: J. Can. Soc. Expl. Geophys., v. 20, 55-59.